Organization of Well-Defined Amphiphilic Graft Copolymers at the Air−Water Interface

Aline F. Miller and Randal W. Richards*

Interdisciplinary Research Centre in Polymer Science and Technology, University of Durham, DURHAM DH1 3LE, U.K.

John R. P. Webster

ISIS Science Division, Rutherford Appleton Laboratory, Chilton, DIDCOT OX1 OQZ, U.K.

Received February 3, 2000; Revised Manuscript Received July 5, 2000

ABSTRACT: A well-defined graft copolymer with a polynorbornene backbone and poly(ethylene oxide) grafts has been spread at the air−water interface and the organization of the copolymer investigated over a wide range of surface concentration using neutron reflectometry. The data have been analyzed using both optical matrix and kinematic approximation methods to provide the dimensions of the regions occupied by the backbone, poly(ethylene oxide) grafts and the near surface water layer thickness. The backbone region has a constant thickness of ca. 5 Å over the whole surface concentration range explored whereas the poly(ethylene oxide) graft layer increases in thickness monotonically over the same surface concentration range from ca. 15 to 45 Å. A more detailed examination of the reflectivity due to the poly(ethylene oxide) layers suggests that it is composed of two layers, one of which has a uniform density of ethylene oxide segments with the second having a parabolic decay of segments. The exponent for the dependence of the poly(ethylene oxide) total layer thickness on the density of grafting of the water surface (σ) was 0.66, i.e., much stronger than predicted by theory for a brush like layer. The near surface water layer self-partial structure factor could not be fitted with the often used uniform layer model. Attempts to model this parameter using multiple uniform layer models or a parabolic increase in water number density could not reproduce the features observed experimentally, suggesting that the near surface water layer is organized in a more complex manner than hitherto suspected when in the presence of poly(ethylene oxide).

Introduction

Small amounts of amphiphilic polymers spread at the air−water interface can have a profound effect on the long-wavelength dynamics of the interface, i.e., the capillary wave phenomena.[1−5] The observed surface viscoelastic properties exhibit a wide variation in behavior dependent on the nature of the spread thin polymer film. This behavior is, to some extent, identifiable with the nature of the polymer and by implication the manner in which the polymer organizes at the air−water interface. Understanding the factors that determine this organization within such thin spread films and by corollary the "structuring" of the near surface water layer is germane to several areas of application. Among these are emulsion stability, film-forming processes, transport across membranes, and preparation of thin film devices on the nanometer length scale.

Quantifying the length scales involved in thin films at fluid interfaces and, more particularly, the distribution of the various species relative to each other calls for sensitive methods because the amounts of polymer involved are generally of the order of micrograms. FTIR has been used to determine the orientation of groups in the polymer with respect to the fluid surface[6] and ellipsometry in conjunction with Brewster angle microscopy[7] can provide some information about "in plane" structures. Insight into the organization normal to the fluid surface is essentially confined to neutron reflectometry[8] although in favorable circumstances X-ray reflectometry[9] can also provide similar information but without the detail accessible to neutron reflectometry using contrast variation.

In the past we have discussed the organization and surface viscoelastic properties of spread films at the air−water interface of a graft copolymer with a poly(methyl methacrylate) backbone and poly(ethylene oxide) (PEO) grafts.[1,10] Unique surface viscoelastic phenomena were exhibited by this graft copolymer, and it was speculated that this may have been due to the grafts having a brush like organization in the aqueous subphase. However, the grafting of the backbone was random, and although the PEO grafts were all of the same degree of polymerization, the grafting density along the backbone could not be controlled. To address this uncertainty we report here the organization at the air−water interface of a well-defined graft copolymer with a hydrocarbon backbone and PEO grafts at every monomer unit in the backbone. A précis of the theory underlying the neutron reflectometry data interpretation is given before the synthetic aspects of the copolymer preparation are described. Surface pressure isotherms precede the neutron reflectometry that are subsequently analyzed by an exact method and the potentially more powerful (in terms of insight obtainable in principle) kinematic approximation.

Theory of Neutron Reflectometry

A brief outline of the theory pertinent to the analysis of the experimental data is presented here. Detailed descriptions of the technique specific to polymer bearing interfaces have been published elsewhere.[11,12] We outline here the exact optical matrix approach and the use of the kinematic approximation.

* To whom correspondence should be addressed.

10.1021/ma000205s CCC: $19.00
Published on Web 09/08/2000

Optical Matrix Description.[13] We are concerned only with the specular reflection of a neutron beam that is incident on an interface. The variation of the reflectivity (= ratio of reflected intensity to incident intensity) with scattering vector Q ($Q = |\mathbf{Q}| = 4\pi(\sin\theta)/\lambda$, where θ is the grazing incidence angle at the interface of neutron beam of wavelength λ) is determined by the change in neutron refractive index normal to the interface. This variation of refractive index can be modeled as a series of lamellae wherein the neutron refractive index is constant but differs from lamella to lamella in a manner depending on the composition distribution normal to the interface. The neutron refractive index is controlled by the scattering length density, ρ, and $\rho = \sum_i n_i b_i$ where n and b are the number density of species i with a coherent scattering length of b. The reflection properties of each stratified layer that models the composition distribution are contained within a characteristic optical matrix and multiplication of all of these matrices for each layer produces an overall matrix from which the reflectivity can be calculated. In applying this approach to the analysis of reflectivity data, one uses the minimum number of layers needed to produce an acceptable fit to the data by varying the thickness and scattering length density of each layer. From the values of these latter two parameters, the composition of each layer can be obtained.

Partial Structure Factor Description. Neutron reflectivity data may be analyzed, under appropriate conditions using the kinematic approximation.[14,15] The layer thickness and number density of the individual species present in the near surface region are provided, but in addition the separation of the layers relative to each other is obtainable. With the condition of weak reflectivity (generally $< 10^{-3}$), and $Q \gg Q_c$ (Q_c being the critical value below which total reflection is observed) then the reflectivity can be expressed as

$$R(Q) = \frac{16\pi^2}{Q^2}|\rho(Q)|^2 \tag{1}$$

where $\rho(Q)$ is the one-dimensional Fourier transform of $\rho(z)$, the scattering length density distribution normal to the interface

$$R(Q) = \left(\frac{16\pi^2}{Q^2}\right)\sum_i\sum_j b_i b_j h_{ij}(Q) \tag{2}$$

where $h_{ij}(Q)$ is the partial structure factor. When $i = j$ the self-partial structure factor is obtained, which contains information on the composition and distribution of the component i and is given by

$$h_{ii}(Q) = |n_i(Q)|^2 \tag{3}$$

with $n_i(Q)$ being the one-dimensional number density distribution of the species i in Fourier space normal to the interface. When $i \neq j$, then the partial structure factor is descriptive of the relative positions of species i and j to each other

$$h_{ij}(Q) = h_{ji}(Q) = \mathrm{Re}[n_i(Q)n_j^*(Q)] \tag{4}$$

where $h_{ij}(Q)$ is the cross partial structure factor.

For a copolymer with different species, A and B spread as a film on water (W), the reflectivity in terms of partial structure factors is given by

$$R(Q) = \frac{16\pi^2}{Q^2}(b_A{}^2 h_{AA} + b_B{}^2 h_{BB} + b_W{}^2 h_{WW} + 2b_A b_B h_{AB} + 2b_A b_W h_{AW} + 2b_B b_W h_{BW}) \tag{5}$$

where A, B, and W denote the individual copolymer components and water, respectively. There are six partial structure factors in eq 5. Therefore, to elucidate the complete near surface organization, six different polymer/subphase contrasts are required. This can be achieved by replacing hydrogenous polymers by deuterated versions and using two subphases, D_2O and null reflecting water (nrw, light and heavy water mixed to give a scattering length density of zero). However, synthetic difficulties may prevent all contrast combinations being obtained. Partial structure factors obtained are then interpreted by applying models for the distribution of the particular species, e.g., a uniform layer or a Gaussian distribution etc.

Experimental Section

General Data. All manipulations of air- and moisture-sensitive materials were performed using standard Schlenk and cannular transfer techniques under vacuum or nitrogen atmosphere or in a glovebox. NMR spectra were recorded using a Varian VXR400S (^{1}H at 399.95 MHz and ^{13}C at 100.58 MHz) using tetramethyl-silane (TMS) as internal standard. Size exclusion chromatography (SEC) data were obtained using chloroform solutions, the instrument being calibrated by poly(ethylene oxide) (PEO) standards of molecular weight ranging from 1000 to 2×10^6 g mol^{-1}.

Materials. Ethylene oxide (EO, hydrogenous and deuterated) (Aldrich) monomer was purified by stirring over sodium hydroxide (24 h), dried over calcium hydride (24 h), and then stirred with 20% v/v of dibutylmagnesium before vacuum distilling immediately prior to use. Hydroxymethyl-5-bicyclo-[2,2,1]heptene (NBMeOH) (Aldrich) was fractionally distilled under reduced pressure (324 K, 0.8 mbar) from molecular sieves and used without further purification. The initiator for the ring opening metathesis polymerization (ROMP) was $RuCl_2(=CHPh)(PCy_3)_2$, (Grubbs initiator) prepared following the published method.[16] Acetic acid and ethyl vinyl ether were used without further purification. Deuterated solvents were stirred over the appropriate drying agent and vacuum distilled prior to use. Solvents used for polymerization reactions were dried by prolonged reflux over the appropriate drying agent (as indicated in parentheses below), freshly distilled and then degassed prior to use: tetrahydrofuran (THF) (potassium benzophenone), benzene (calcium hydride), and chloroform (phosphorus pentoxide).

Synthesis. Graft copolymers were prepared by a two-stage process; first synthesis of a macromer and second the ROMPing of this macromer to produce the final copolymer. The same procedures were used for both the hydrogenous and part deuterated graft copolymers except that ^{1}H NMR was omitted for the latter.

Macromer Preparation.[17] Typically, 3.85 mmol of a 1 M stock solution of NBMeOH was added to 100 mL of dry, degassed THF in a previously evacuated vessel (10^{-7}mbar). This solution was cannulated under positive dry nitrogen pressure on to a potassium mirror in an evacuated vessel and allowed to deprotonate for 24 h before being transferred back to a freshly cleaned vessel. This initiating solution was subjected to repeated freeze, evacuate, and thaw cycles before the calculated quantity, 0.114 mol, of EO was vacuum distilled into the THF solution of the metalated NBMeOH. The solution was stirred continuously at room temperature for 3 days before terminating the living chain ends by adding excess degassed glacial acetic acid. The macromer was recovered by precipitation in a 10-fold excess of chilled hexane. After filtration and drying under vacuum at 298 K for 3 days, the white powder obtained was analyzed by SEC, viscometry, and ^{1}H and ^{13}C

Table 1. Molar Mass, Polydispersity, and Intrinsic Viscosities for Macromers and Copolymers

	macromer		graft copolymer	
	hydrogenated	deuterated	hydrogenated	deuterated
molecular weight	1300	1300	63400[a]	66200[a]
polydispersity	1.09	1.11	1.26	1.29
intrinsic viscosity/g cm^{-3}	8.7	8.8	30.6	30.8

[a] Estimated from molecular weight of macromer

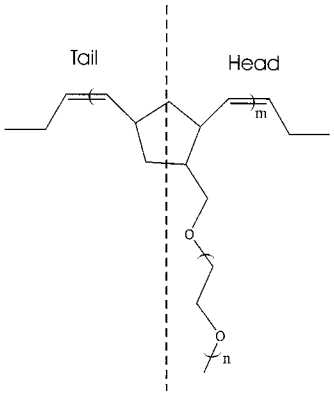

Figure 1. Schematic structure of poly(norbornene)-*g*-poly(ethylene) oxide copolymer.

NMR. Analysis of the NMR spectra indicated that the number of ethylene oxide segments per molecule was 27 ± 2, in close agreement with results from SEC that indicated a degree of polymerization of 26 ethylene oxide units with a polydispersity of 1.09. This macromer was used without further purification.

Graft Copolymer Synthesis.[17,18] Typically a 5 mL solution of the Grubbs catalyst (47 μmol) in dry, degassed benzene was added to a 20 mL solution (2.3 mmol) of the prepared macromer (M_n = 1300 g/mol) in benzene. This was stirred vigorously for 4 days before the ruthenium complex was cleaved from the chain ends by adding excess ethyl vinyl ether. The copolymer was precipitated in a 10-fold excess of chilled diethyl ether, isolated, and dried. Repeated dissolution and precipitation of the copolymer in the minimal volume of benzene removed residual catalyst finally producing a white powder after drying under vacuum at 298 K. The absence of characteristic resonances for the macromer from the NMR spectrum of the polymer demonstrated that all the macromer had been incorporated into graft copolymer. Because of the high content of PEO in the graft copolymer the hydrodynamic properties of the graft copolymer are similar to that of the macromer, and both elute from the SEC column at a similar elution volume. The SEC data was monomodal with a slightly broader polydispersity of 1.26 compared to that of the macromer. Confirmation that ROMP was successful was obtained by comparing the intrinsic viscosities of the macromer and graft copolymers in chloroform solution at 298 K. The intrinsic viscosity of the graft copolymers was ca. 3−4 times that of the macromer from which it was prepared. The intrinsic viscosities and molecular weights of each species are given in Table 1. The similarity of the intrinsic viscosities for the hydrogenous and deuterated materials (macromer and copolymer) indicates they have very similar molecular weights.[19]

A schematic of the graft copolymer is shown in Figure 1. We discuss here the fully hydrogenous (hn25) and the part-deuterated (dn25) counterpart (where only the PEO grafts were deuterated) with $n \approx 25$ and $m \approx 50$. Evidence for the existence of both cis and trans double bonds was noted in the ^{1}H NMR spectra of the polymers.[20] Because resonances for protons on the doubly bonded carbons were close together and the signal-to-noise ratio was low, precise cis/trans content could not be calculated but was estimated to be 33% cis and 67% trans. The copolymers also contain a mixture of tacticities depending on the orientation of each macromer to the propagating species at the instant of polymerization. If we arbitrarily label the PEO containing part of the macromer as the head (H), and the remainder as the tail (T), it was estimated that 39% of the cis bonds were HH or HT additions, 51% were TH, and 9% TT. For trans bonds the percentages of the various additions were estimated as 7% HH, 15% TH, 26% HT and 52% TT.

Surface Pressure Isotherms. Surface pressure−surface concentration isotherms at 298 K for PEO homopolymer and each graft copolymer were obtained using a NIMA (Coventry, U.K.) Langmuir trough, model 2001. The trough was mounted on a vibration isolation table and the subphase temperature regulated by circulating water from an external thermostat, through the poly(tetrafluoroethylene) base of the trough. Typically 20 μL of a 1.0 mg mL^{-1} chloroform solution of the copolymers was deposited dropwise onto the surface of freshly aspirated, ultrahigh quality water (Elgastat UHQ). The system was left for 20 min to allow evaporation of solvent and for the film to reach the equilibrium state. The film was then compressed at a rate of 30 cm^2 min^{-1} from an initial area of 900 cm^2 to 80 cm^2 recording the surface pressure continuously.

Neutron Reflectometry. Neutron reflectometry (NR) data were obtained using both CRISP and SURF reflectometers at the UK pulsed neutron source, ISIS, at the Rutherford Appleton Laboratory, Didcot, Oxfordshire, England. The momentum transfer range used was $0.02 \leq Q/Å^{-1} \leq 0.6$. A rectangular NIMA trough was mounted on an antivibration table and enclosed by a Perspex box to prevent H/D exchange between subphase and atmosphere. The well-collimated neutron beam entered and exited the enclosing box via quartz windows. Reflectivities were placed on an absolute scale by calibration using a clean D_2O subphase. Three combinations of copolymer and subphase were used: fully hydrogenous copolymer on D_2O, part deuterated copolymer on D_2O, and part deuterated copolymer on nrw.

Results

Surface Pressure Isotherms. Surface pressure isotherms for the hydrogenous graft copolymer and homo PEO are compared in Figure 2a, and clear differences between the spread films are evident. The surface pressure of homo PEO rises quickly from ca. 0.1mN m^{-1} at a surface concentration of ∼0.1 mg m^{-2} and reaches an equilibrium surface pressure of 10mN m^{-1} at ca. 0.6 mg m^{-2}. At this surface concentration it has been shown that the number density of PEO segments of the uppermost layer is constant,[21] and the PEO chains start to extend into the subphase as loops and tails at higher surface concentrations. At low surface concentrations (Γ_s), the isotherm of the graft copolymer behaves in a manner similar to homo PEO. A steep rise in the surface pressure is observed over a narrow surface concentration range (0.2−0.7 mg m^{-2}); thereafter, the increase in surface pressure is reduced, and an asymptotic surface pressure of ca. 16 mN m^{-1} appears to be approached. The different isotherm behavior for copolymer and homopolymer suggests that the monolayer organization of the two polymers differs.

For the neutron reflectometry experiments it was important to verify that (a) there was no influence of replacing hydrogenous ethylene oxide by deutero ethylene oxide and (b) the spread films were stable over the time required to collect reflectivity data. Isotherms for the part deuterated and hydrogenous graft copoly-

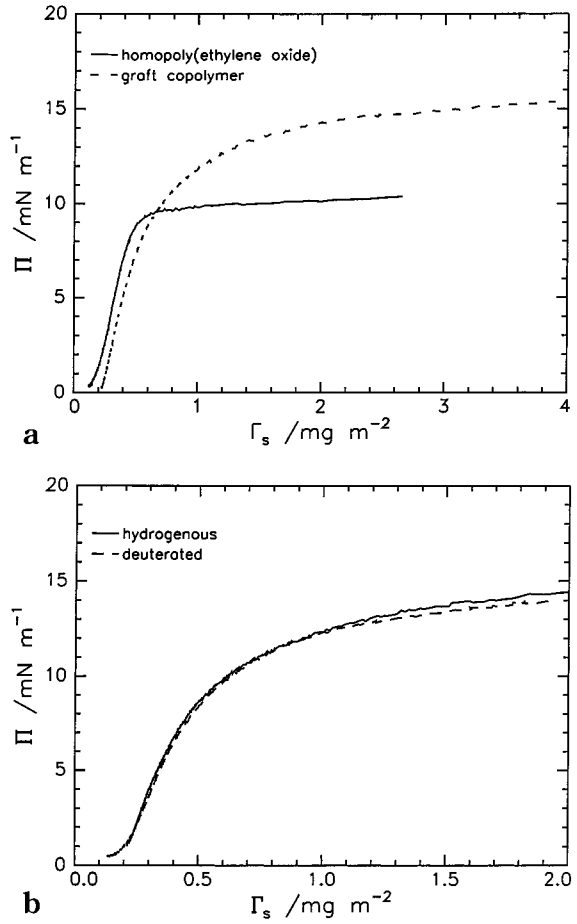

Figure 2. (a) Surface pressure isotherms for homopoly(ethylene oxide) and the graft copolymer at 298 K. (b) Surface pressure isotherms for hydrogenous and part deuterated graft copolymers.

mers are compared in Figure 2b. The differences are negligible, and isotopic substitution has no effect on the thermodynamic properties (as sampled in the surface pressure isotherm), and there is no significant difference in spread film organization between the two isotopic isomers of the graft copolymer. To confirm that the spread films retained a stable conformation over a prolonged period, the surface pressure of freshly spread monolayers with Γ_s values of 0.5, 1.0, and 2.0 mg m^{-2} were continuously monitored for times in excess of 4 h. A small relaxation takes place after the initial compression to the desired surface concentration, thereafter the surface pressure remains constant with increased time; i.e., the surface organization of the copolymers was stable with no dissolution into the subphase.

Neutron Reflectometry. Reflectivity profiles have been obtained for seven separate surface concentrations of each isotopic contrast between copolymer and subphase (dn25 on nrw; hn25 and dn25 on D_2O). Figure 3 shows selected reflectivity profiles for copolymer dn25 on nrw. As expected the reflectivity increases with surface concentration due to the increase in deuterated PEO in the near surface because it is essentially the only source of reflectivity for this copolymer-subphase combination. For copolymers spread on D_2O, the reflectivity of the subphase is dominant and the changes due to the presence of a polymer can be elusive. This is evident in Figure 4 where reflectivities obtained for dn25 and hn25 at a surface concentration of 2.0 mg m^{-2} spread on D_2O are compared to that for D_2O alone. The

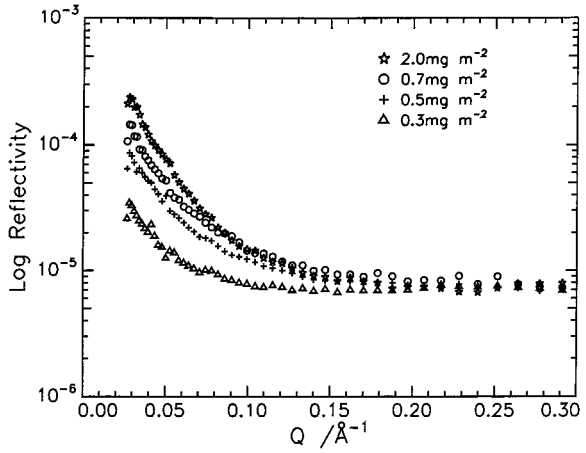

Figure 3. Reflectivity data for a range of surface concentrations for the part deuterated copolymer on nrw.

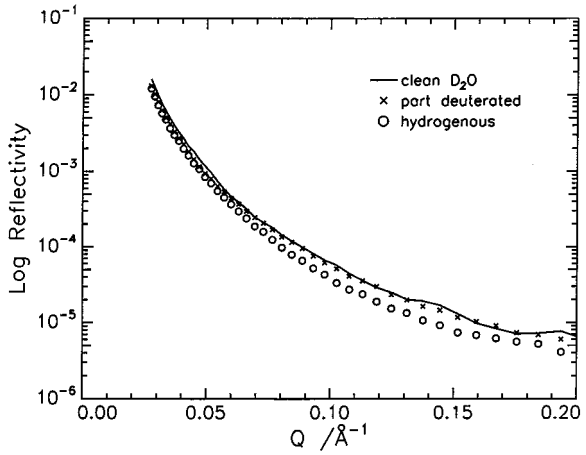

Figure 4. Reflectivity profiles for clean D_2O and the hn25 and dn25 copolymers spread on D_2O at a surface concentration of 2.0 mg m^{-2}.

reflectivity for the dn25/D_2O combination is very similar to that of the D_2O subphase because the small percentage of hydrogenous backbone present produces an almost negligible reduction in the reflectivity. When the spread copolymer is fully hydrogenous, there is a more distinct reduction from the reflectivity of pure D_2O. Even though the effects of the spread layer on D_2O are rather more subtle than with an nrw subphase, the influence of a hydrogenous spread film is evident even at low values of Γ_s, Figure 5. The immediate surface layer clearly contains more hydrogenous polymer as the surface concentration increases.

Discussion

Surface Pressure Isotherms. Extrapolation of the low concentration linear portions of the surface pressure isotherms for the graft copolymers to zero surface concentration gives their limiting areas. For both part-deuterated and the hydrogenous graft copolymers this limiting area is identical at ca. 5×10^{23} Å^2 g^{-1}. This value is marginally smaller than that for the spread film of poly(ethylene oxide) i.e., 5.88×10^{23} Å^2 g^{-1}. The similarity of these two values for polymers that are very different in their molecular structure suggests that the content of EO segments in the surface layer is similar notwithstanding the different architecture of the two polymers. The scaling law exponents[22−24] for the relation between surface pressure and surface concentration, i.e.,

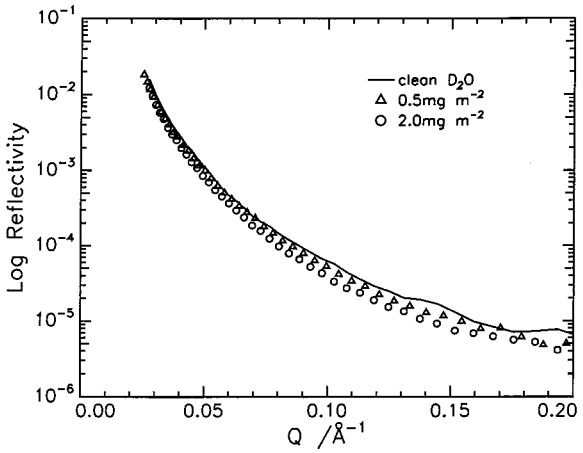

Figure 5. Influence of surface concentration on reflectivity for hn25 spread on D_2O.

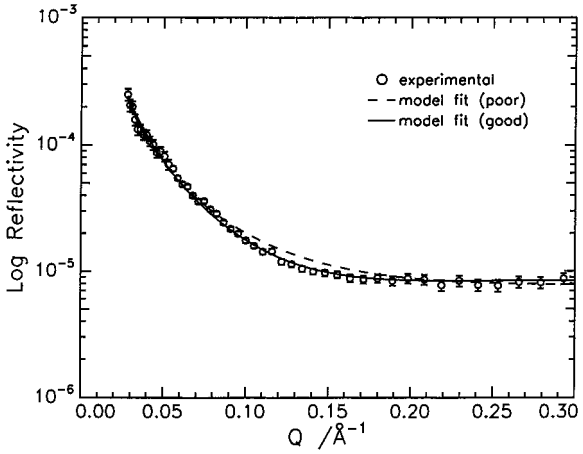

Figure 6. Fits of single and three layer models to experimental reflectivity data for the part deuterated copolymer on nrw for $\Gamma_s = 2.0$ mg m^{-2}.

$\pi = \Gamma_s^y$, where $y = 2\upsilon/(2\upsilon - 1)$ and υ is the excluded volume exponent, the value of which reflects the nature of the thermodynamic interaction between polymer and subphase. The value of υ obtained for the copolymers (again from the linear surface pressure data region) was 0.68, very close to the value of 0.75 for spread films of PEO on water,[21] indicative of thermodynamically favorable conditions and no significant differences between the interactions of the two copolymers with the aqueous subphase. Evidently the presence of the hydrocarbon backbone is not too detrimental for the thermodynamics of the aqueous subphase-graft copolymer interaction. A note of caution should be made here, because the interpretation of the scaling law exponents is strictly only valid for spread films of homopolymers.

Neutron Reflectometry Data. Quantitative descriptions of the spread copolymer films have been obtained using the two methods outlined earlier: the optical matrix and kinematic approximation methods. Application of a complete analysis using the kinematic approximation analysis was not possible, because the copolymer backbone is unavailable in a fully (or even part) deuterated form; consequently, a simplified kinematic approximation has been applied.

Optical Matrix Analysis. Initially, a single uniform layer model with layer thickness, d, and scattering length density, ρ, was applied and the calculated reflectivity nonlinearly least-squares fitted to the experimental data by adjusting d and ρ. From these best-fit values, parameters describing the near surface organization were obtained. The scattering length density for such a uniform layer is the sum of the individual contributions

$$\rho = \sum n_i b_i \tag{6}$$

where n_i is the number density and b_i the coherent scattering length of species i, the latter being tabulated in Table 2. From values of n_i the surface concentration, Γ_s, can be calculated for each of the species in the layer

$$\Gamma_s = \frac{n_i m_i d}{N_A} \times 10^{20} \text{ mg m}^{-2} \tag{7}$$

where m_i is the molecular weight of species i and N_A is Avogadro's number.

Table 2. Scattering Length and Scattering Length Densities

unit	$\sum b_i/10^{-4}$ Å	$\rho/10^{-6}$ Å^{-2}
H_2O	−1.68	−0.56
D_2O	1.92	6.35
air	0	0
ethylene oxide	0.41	0.56
deuterated ethylene oxide	4.58	6.33
norbornene	1.78	0.89

A single uniform layer did not produce an acceptable fit to any of the data, and additional uniform layers were therefore incorporated. To overcome any uncertainty about the uniqueness of the model used to fit the data, reflectivity curves for all three polymer−subphase contrasts used were fitted concurrently using the same model. Consistency of layer dimensions was used as a criterion for the validity of a model for the spread polymer organization. Furthermore, a model was only accepted if the surface concentrations calculated from the fit parameters were in good agreement with the actual amount of copolymer spread.

A typical one layer fit [labeled model fit (poor)] is shown in Figure 6 for graft copolymer dn25 on nrw. Clearly, this model fails to reproduce the data well; moreover, the surface concentration of the copolymer calculated from the fit parameters is only 63% of the spread amount. A three-layer model [labeled model fit (good) in Figure 6] gave an excellent fit to the experimental reflectivity data, layer dimensions for all contrasts were identical within experimental error, and the calculated surface concentrations were in acceptable agreement with the amount of copolymer spread. Exact agreement between calculated and experimental surface concentrations for the PEO grafts was never obtained, a point we return to later. The thickness, volume fraction composition (from $\rho = \sum_i \phi_i \rho_i$) and number density of EO segments of the individual layers for all surface concentrations investigated are given in Table 3 and volume fraction profiles normal to the surface for selected surface concentrations are shown in Figure 7. Table 4 compares the surface concentrations of PEO calculated from the fits to the reflectivity data with the actual amount in the surface region.

From the scattering length densities obtained for each of the layers, we conclude that the hydrophobic backbone is predominantly in the air phase and forms the uppermost layer with the hydrophilic grafts penetrating

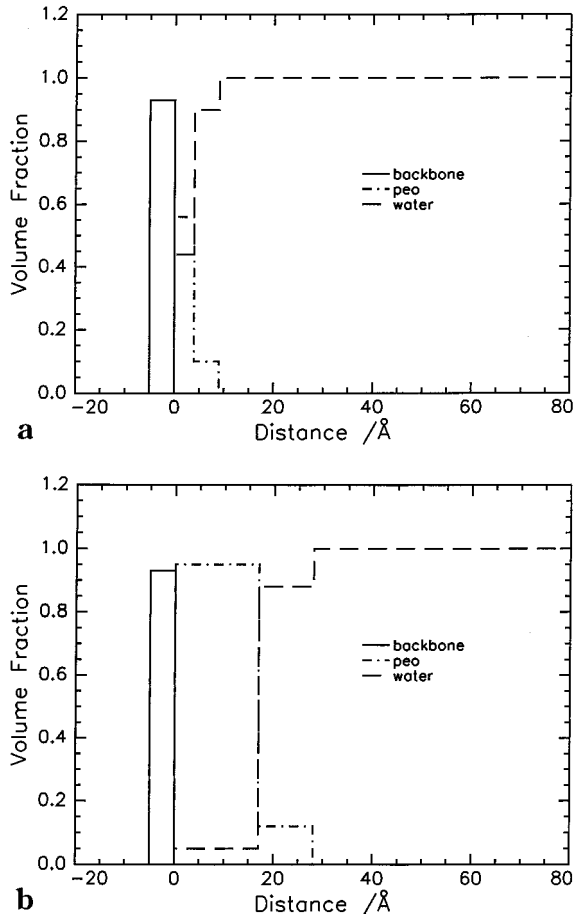

Figure 7. Volume fraction profile for the three-layer model at Γ_s values of a) 0.3 mg m^{-2} and (b) 2.0 mg m^{-2}.

Table 3. Volume Fraction Compositions and Layer Thicknesses from Optical Matrix Analysis of Neutron Reflectometry Data Using Three Uniform Layers

Γ_s/mg m^{-2}	layer	d/Å	ϕ_{NB}	ϕ_W	ϕ_{EO}	ϕ_{AIR}	$n_{NB}/10^{-3}$ Å^{-3}	$n_{EO}/10^{-3}$ Å^{-3}
2.0	1	4 ± 0.5	0.44	0.00	0	0.56	2.20	
	2	17 ± 0.5	0	0.09	0.91	0		12.56
	3	11 ± 0.5	0	0.88	0.12	0		1.66
1.5	1	4 ± 1.0	0.60	0	0	0.40	3.00	
	2	16 ± 1.0	0	0.19	0.81	0		11.18
	3	8 ± 0.5	0	0.84	0.16	0		2.21
1.0	1	4 ± 0.5	0.97	0	0	0.03	4.85	
	2	13 ± 0.5	0	0.37	0.63	0		8.69
	3	7 ± 1.0	0	0.95	0.05	0		0.69
0.7	1	4 ± 0.5	0.73	0	0	0.27	3.65	
	2	10 ± 1.0	0	0.43	0.57	0		7.87
	3	6 ± 0.5	0	0.96	0.04	0		0.55
0.5	1	4 ± 0.5	0.89	0	0	0.11	4.45	
	2	7 ± 0.5	0	0.44	0.56	0		7.73
	3	7 ± 0.5	0	0.96	0.04	0		0.55
0.4	1	4 ± 0.5	0.89	0	0	0.11	4.45	
	2	4 ± 0.5	0	0.36	0.64	0		8.83
	3	6 ± 1.0	0	0.86	0.14	0		1.93
0.3	1	3 ± 0.5	0.93	0	0	0.07	4.65	
	2	3 ± 0.5	0	0.44	0.56	0		7.73
	3	5 ± 0.5	0	0.92	0.08	0		1.10

the aqueous subphase. This uppermost layer containing chiefly the hydrocarbon backbone and air is confined to a thin 3−5 Å layer over the entire range of Γ_s investigated. The volume fraction of the air included in this layer increases, albeit with no discernible regularity, as the monolayer is compressed. This increased air content may be due to some "buckling" of the single bond regions of the hydrocarbon backbone out of the plane of the aqueous subphase surface as the film is compressed. Evidently this cannot lead to a large increase in the spatial dimensions occupied by the backbone since none is observed. Molecular modeling[25] of the backbone alone shows that it adopts a helical structure when compressed at the ends of the chains; this may be occurring in the thin spread films, and hence we would not anticipate any marked change in the dimensions of the layer. However, we note that the scattering length density of the backbone is low and neutron reflectometry will not be very sensitive to small changes in the dimensions of this layer. An additional aspect relates to the earlier remarks concerning the copolymer backbone stereochemistry. For all the PEO grafts to penetrate the aqueous subphase a proportion of the grafted PEO chains must curl over the backbone. The driving force for this presumably arises from the energy minimization obtained on immersion of the hydrophilic PEO grafts but the quantities of PEO in the backbone region must be very small since the scattering length density is very low for all contrasts. The two uniform layers contain only PEO and water. Layer 2 (see Table 3) contains a high volume fraction of PEO in comparison to layer 3, indicative of the dilution of the free ends of the grafts as they penetrate deeper into the subphase. As the surface concentration increases, the thickness of layer 2 increases steadily and while the thickness of the third layer does not increase regularly, there is nevertheless an overall increase. The composition of these PEO containing layers changes on compression, that of layer 2 increasing in PEO content from a volume fraction of 0.56−0.91 as surface concentration increases from 0.3 to 2.0 mg m^{-2}, most of this increase occurring for $\Gamma_s \geq 1.0$ mg m^{-2}. The PEO content of layer 3 increases in a likewise manner. The changes in the overall dimensions of the PEO containing layers are discussed later.

Table 4. Calculated Surface Concentrations of PEO from the Three Uniform Layer Model

Γ_{sTOTAL}/mg m^{-2}	Γ_{sEO}/mg m^{-2}	$\Gamma_{s\ EO\ cal}$/mg m^{-2}	$\Gamma_{sEO}/\Gamma_{s\ EO\ cal}$
2.0	1.82	1.75 ± 0.08	0.96
1.5	1.37	1.33 ± 0.17	0.97
1.0	0.91	0.86 ± 0.10	0.94
0.7	0.64	0.63 ± 0.10	0.98
0.5	0.46	0.46 ± 0.08	1.00
0.4	0.36	0.35 ± 0.09	0.97
0.3	0.27	0.27 ± 0.08	1.00

Kinematic Approximation Analysis. The good agreement between calculated and actual surface concentrations and the physically acceptable description of optical matrix analysis notwithstanding, the kinematic approximation was also applied to the neutron reflectometry data for two reasons. First, the distributions of copolymer and water in the near surface region are separately obtainable; second, the separation between these two distributions becomes accessible in principle. However, because of the unavailability of the backbone in a deuterated form, we can only use a subset of the relations available, and moreover, we have to assume that the hydrogenous copolymer (or the hydrogenous parts of the copolymer) do not contribute to the reflectivity. The latter is not too drastic an assumption because both backbone and hydrogenous PEO have low scattering length densities (Table 2). Hence, for the part deuterated copolymer spread on nrw, we can write the reflectivity as

$$R(Q) = \frac{16\pi^2}{Q^2} b_E{}^2 h_{EE} \tag{8}$$

where E represents ethylene oxide.

For the fully hydrogenous copolymer spread on D_2O, assuming that the contribution to the specular reflection from the copolymer is zero

$$R(Q) = \frac{16\pi^2}{Q^2} b_w{}^2 h_{ww} \tag{9}$$

where w represents water.

Background contributions were subtracted, and for reflectivity data obtained where D_2O was the subphase, the correction procedure of Crowley et al.[26] was applied before expressing the data in terms of partial structure factors. Figure 8 shows background-subtracted data for the part deuterated copolymer on nrw as the derivatives of the PEO self-partial structure factors ($\equiv Q^4R(Q)/16\pi^2b^2$), because presenting the data in this way is more informative.[8,11] Two models have been used to interpret these data: first a half Gaussian distribution of EO segments normal to the surface and second a composite model with the EO segments distributed over a uniform layer with an added parabolic decay.

For the half Gaussian distribution the real space distribution is

$$n_i(z) = n_{il} \exp\left(\frac{-4z^2}{\sigma^2}\right)$$

the partial structure factor is given by

$$h_{ii}(Q) = (n_i{}^2)\left(\frac{\pi\sigma^2}{4}\right) \exp\left(\frac{-Q^2\sigma^2}{8}\right)$$

where n_i is the number density of PEO segments at the air−water interface and σ is the standard deviation of the half Gaussian layer. The surface concentration for such a distribution is

$$\Gamma_s = \left(\frac{4}{3} n_i \sigma\right) \frac{m_i}{N_A} \times 10^{-23} \text{ mg m}^{-2}$$

For the case where the segments are distributed in a uniform plus parabolic layer, the real space distribution is (Figure 9 shows a sketch of the distribution)

$$n_i(z) = 0 \quad z \le -\sigma - \epsilon$$

$$n_i(z) = n_{i2}\left(1 - \frac{(z+\sigma)^2}{\epsilon^2}\right) \quad -\sigma - \epsilon \le z \le 0$$

$$n_i(z) = n_{i1} \quad -\sigma \le z \le 0$$

$$n_i(z) = 0 \quad z > 0$$

the partial structure factor is given by

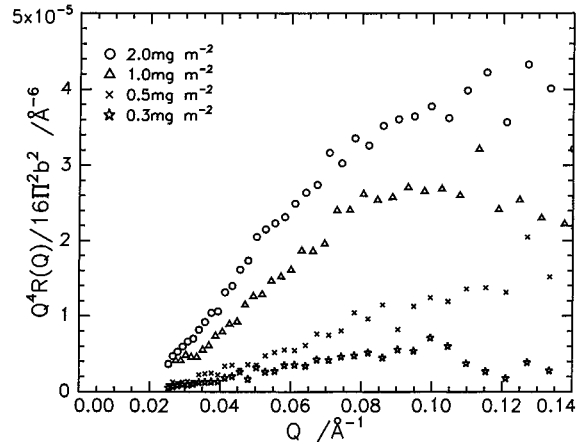

Figure 8. PEO self-partial structure factors, (in the derivative form) for different Γ_s values spread on nrw.

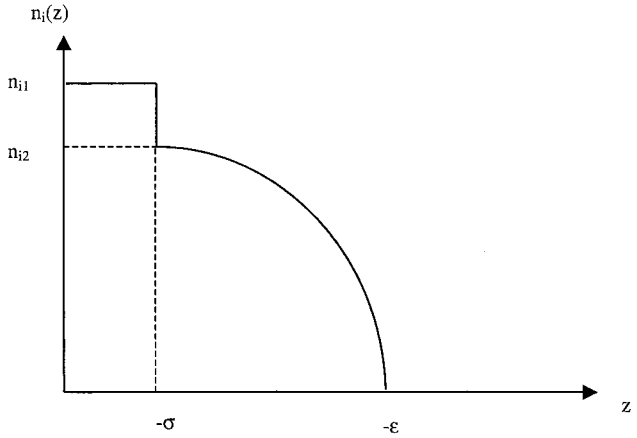

Figure 9. Schematic sketch of uniform layer plus parabolic decay distribution of segments.

$$h_{ii}(Q) = 2n_{i1}{}^2 + n_{i2}{}^2 - 2n_{i1}n_{i2} + 2n_{i1}\cos(Q\sigma)[n_{i2} - n_{i1}] + \frac{1}{Q^2\epsilon^4}\{8n_{i2}{}^2[1 + Q^2\epsilon^2] + [\cos(Q\epsilon) + Q\epsilon \sin(Q\epsilon)][4n_{i1}n_{i2}Q^2\epsilon^2 - 4n_{i2}{}^2Q^2\epsilon^2 - 8n_{i2}{}^2] + 4n_{i1}n_{i2}Q^2\epsilon^2[\cos(Q\sigma) - \cos(Q(\sigma+\epsilon)) - Q\epsilon\, sin(Q(\sigma+\epsilon)) - 1]\}$$

for which the surface concentration is

$$\Gamma_s = \left(n_{i1}\sigma + \frac{2n_{i2}\epsilon}{3}\right) \frac{m_i}{N_A} \times 10^{-23} \text{mg m}^{-2}$$

where n_{i1} and n_{i2} are the number densities of the uniform and parabolic layer respectively, while σ and ϵ are the thickness of the uniform and parabolic layers, respectively.

The parameters of these models (n_{i1} and σ for the Gaussian, n_{i1}, n_{i2}, σ, and ϵ for the uniform layer with added parabolic decay) were the adjustable fitting parameters for the nonlinear least-squares fit to the data. Examples of typical fits for each case are shown in Figure 10, and over this Q range both functions fit the data equally well. Distinction between the two possible models only becomes evident at higher Q values; unfortunately, the background contribution to the total reflectivity overwhelms any content from the layer organization at these higher Q values. Surface concentrations and layer thicknesses have been calcu-

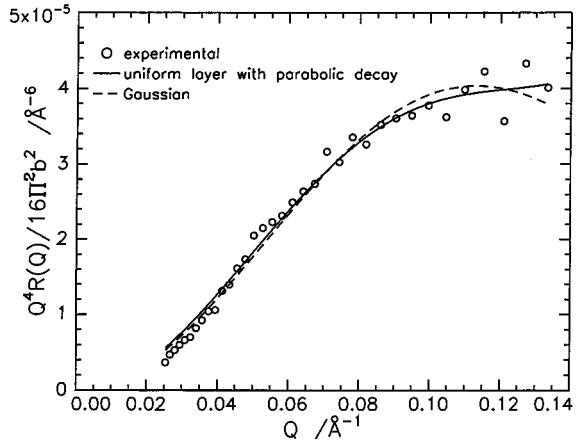

Figure 10. PEO self-partial structure factors of the half-Gaussian model and uniform layer plus parabolic decay fitted to neutron reflectivity data.

lated for the Gaussian distribution and uniform layer plus parabolic decay models using their individual characteristic parameters. Layer thicknesses and number densities obtained are given in Tables 5 and 6, respectively. Overall, the surface concentration of PEO from the uniform layer plus parabolic decay model gave the closest agreement to the actual amount of PEO spread on the aqueous subphase. No values are given for the lowest surface concentration spread film, 0.3 mg m^{-2}, because the partial structure factor data were too scattered to have confidence in fitted values. However, the concentration of PEO calculated from the uniform-parabolic layer model is not in satisfactory agreement with the amount actually spread. This may be due to the assumption that hydrogenous parts of the copolymers make a negligible contribution to the reflectivity. To correct for this possibility, the optical matrix approach was used to fit the uniform plus parabolic layer model to the reflectivities for all graft copolymer−subphase combinations. The layer thickness, volume fractions, and surface concentrations obtained from this optical matrix analysis are given in Table 7 and the total thickness of the region occupied by the PEO grafts is compared to the values obtained either by uniform layer models or the kinematic approximation results in Figure 11. The Γ_s values in Table 7 are in good agreement with those calculated from the uniform layer model (Table 4), but we still do not account for all of the PEO. Second, from Figure 11 the PEO occupied region thickness from the uniform layer with parabolic decay using the optical matrix method agree well with those obtained by partial structure factor analysis using the same model.

The best agreement between the actual amounts of copolymer spread and that calculated from fitting to the neutron reflectometry model is obtained using exact optical matrix analysis and the three uniform layers model describing both hydrocarbon backbone and PEO contributions and the uniform layer plus a parabolic decay region for the PEO region alone. In the three-layer model, layers 2 and 3 correspond to the uniform and parabolic decay regions of this latter mode, and it is noteworthy that the number densities for these regions in the two models are rather similar.

Whatever model is adopted to analyze the reflectivity data quantitatively, all show that the PEO layer increases in thickness as the surface concentration of graft copolymer increases. For the degree of polymerization of PEO grafts investigated here, the radius of gyration calculated from relations for PEO of much higher molecular weight in solution would be ca. 22 Å, and the grafts are separated by a distance of ∼ 6 Å along the backbone. There is thus considerable overlap between the PEO grafts along this path; however, the observation of total thickness of PEO layers being much less than 22 Å at low surface concentrations suggests that the PEO is initially adsorbed to the air−water interface aided by some rotation of the main chain backbone. Because of the double bonds in the main chain, an adsorbed conformation equivalent to that of poly(ethylene oxide) cannot be expected. At the lowest surface concentration of 0.3 mg m^{-2}, the area per repeat unit of the polymer is ca. 700 $Å^2$. Allowing for a reduction in the radius of gyration because of incompletely flat adsorption of the PEO grafts at the air−water interface (to an effective value of, e.g., 15 Å), then the surface concentration does not have to increase significantly before the PEO grafts begin to interact, increasing the total free energy. To reduce the free energy of the system, the PEO grafts begin to explore deeper regions of the subphase, but there is an additional drive to stretch deeper because of the close proximity **along** the backbone chain as referred to earlier. Table 3 shows that the influence of this interaction and overlap is evident at surface concentrations between 0.3 and 0.5 mg m^{-2}, and above this concentration the extension to greater depths becomes even more marked. Because the PEO grafts are attached to the backbone (and thus the air−water interface) by one end, a presumption of pseudobrushlike layer behavior appears to be a reasonable approach to adopt in discussing the data. The original Alexander−de Gennes[27,28] brush layer model used a uniform layer to describe the brush with all the ends located at the same distance from the surface. Subsequently, Milner, Witten, and Cates[29,30] developed a theory where the distribution of polymer segments in the layer is parabolic and the ends are distributed over the whole region. In both cases, however the relation between brush layer thickness (h) and grafting density (σ number of grafted polymer chains per unit area) is given by

$$h \propto \sigma^{1/3}$$

Values of σ for the graft copolymer spread films have been calculated from the average number of grafts per molecule using the surface concentration and assuming that every PEO graft is immersed in the subphase. A linear dependence of the PEO layer thickness on the grafting density is clearly evident in the double logarithmic plot of Figure 11 using the PEO layer thickness obtained from all the models used to analyze the reflectivity data. However, the exponent obtained from these data is $^2/_3$ and not the $^1/_3$ predicted by theory, i.e., a much stronger dependence than predicted. We note that there are distinct differences between the theoretical models and the experimental situation that prevails here. Notably, the PEO grafts are of modest molecular weight and thus will have a considerably more stiff, rod like character than the flexible coil characteristics presumed in the theories, thus leading to a more extended layer thickness than anticipated. Second, the theories of the brush layers surrounded by solvent assume the grafts are fixed in their position on the surface. This is almost certainly not true for the PEO grafts in the spread films discussed here; in addition to the capillary wave fluctuations, there may be diffusion

Table 5. Layer Thicknesses, Number Densities and Calculated Surface Concentrations of the PEO Region Modeled as a Uniform Layer with a Parabolic Decay Using Kinematic Approximation Analysis

Γ_s/mg m^{-2}	Γ_{sEO}/mg m^{-2}	d_1/Å	$n_1/10^{-3}$ Å^{-3}	d_2/Å	$n_2/10^{-3}$ Å^{-3}	$\Gamma_{sEO,cal}$/mg m^{-2}	$\Gamma_{sEO,cal}/\Gamma_{sEO}$	tot. thickn/Å
2.0	1.72	8 ± 1	10.22 ± 0.8	34 ± 2	3.14 ± 0.19	1.20	0.70	42
1.5	1.29	6 ± 1	9.03 ± 0.11	35 ± 5	2.75 ± 0.14	0.96	0.75	41
1.0	0.86	6 ± 1	4.26 ± 0.12	30 ± 4	2.98 ± 0.19	0.68	0.79	36
0.7	0.60	6 ± 1.4	3.91 ± 0.10	16 ± 4	2.13 ± 0.43	0.37	0.62	22
0.5	0.43	5 ± 1	4.05 ± 0.20	16 ± 3	1.76 ± 0.18	0.32	0.75	22
0.4	0.35	5 ± 0.5	2.91 ± 0.19	11 ± 3	1.72 ± 0.09	0.22	0.63	16

Subscripts 1 and 2 denote uniform and parabolic layers, respectively.

Table 6. Layer Thicknesses, Number Densities, and Calculated Surface Concentrations of the PEO Region Modeled as a Gaussian Distribution Using Kinematic Approximation Analysis

Γ_s/mg m^{-2}	Γ_{sEO}/mg m^{-2}	d/Å	$n/10^{-3}$ Å^{-3}	$\Gamma_{sEO,\,cal}/\Gamma_{sEO}$
2.0	1.72	28 ± 0.5	4.58 ± 0.03	0.90
1.5	1.29	26 ± 0.5	4.44 ± 0.03	0.82
1.0	0.86	25 ± 0.5	4.41 ± 0.03	0.78
0.7	0.60	26 ± 1	1.60 ± 0.03	0.29
0.5	0.43	20 ± 2	2.66 ± 0.12	0.37
0.4	0.35	26 ± 2	1.32 ± 0.04	0.24

Table 7. Volume Fractions,[a] Layer Thicknesses, and Calculated Surface Concentrations from Optical Matrix Calculations: Uniform Layer Plus Parabolic Decay

Γ_s/mg m^{-2}	d_1/Å	ϕ_1	d_2/Å	ϕ_2	$\Gamma_{sEO\ cal}$/mg m^{-2}	$\Gamma_{sEO}/\Gamma_{sEO\ cal}$
2.0	11 ± 1	0.77	25 ± 1	0.26	1.85 ± 0.12	0.99
1.5	6 ± 2	0.72	24 ± 1	0.24	1.33 ± 0.20	0.98
1.0	11 ± 1	0.58	17 ± 4	0.08	0.91 ± 0.11	1.00
0.7	5 ± 2	0.43	16.5 ± 1	0.15	0.60 ± 0.11	0.95
0.5	5 ± 1	0.61	12 ± 1	0.06	0.44 ± 0.08	0.98
0.4	5 ± 1	0.39	7 ± 1	0.12	0.34 ± 0.06	0.94
0.3	5 ± 1	0.44	4 ± 3	0.06	0.27 ± 0.08	1.00

[a] Subscripts 1 and 2 denote the uniform and parabolic layer, respectively.

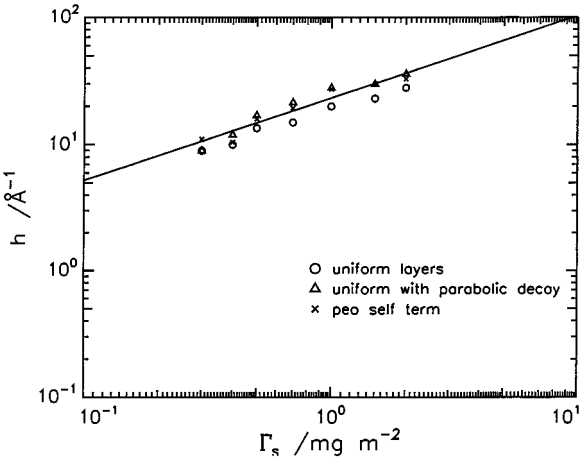

Figure 11. Double logarithmic plot of the PEO layer height as a function of the grafting density of the air−water interface.

in the plane of the water surface, producing regions where the grafting density of the water surface (and hence layer thickness) is higher than in other regions. These more highly grafted regions may be dominant in the reflectivity and the dimensions obtained will be more characteristic of these regions than of the whole spread film.

It is anticipated that the water in the immediate near surface layer may, over a finite spatial range, have a different number density compared to that of the bulk aqueous subphase. This is due to the effects of the spread film and any interactions between the segments

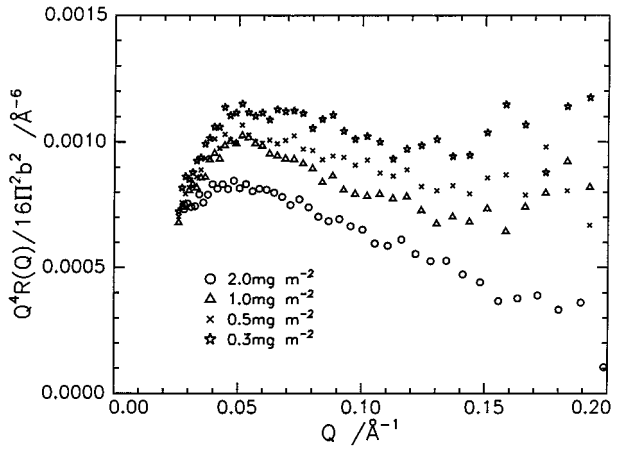

Figure 12. Comparison of neutron data (in kinematic approximation form) for water self-partial structure factor at a range of spread surface concentrations.

of the poly(ethylene oxide) grafts and water. In developing the partial structure factor description of reflectivity from liquid interfaces, Lu et al.[15] proposed a model for the subphase consisting of a finite uniform layer with a lower number density than that of pure water followed by an effectively infinitely thick layer of pure water. The expression for the self-partial structure factor based on the gradient of the water number density normal to the surface is

$$Q^2 h_{ss}(Q) = {n_{s0}}^2 + 4n_{s1}(n_{s1} - n_{s0} \sin^2 (Q\sigma/2))$$

where n_{s0} and n_{s1} are the number densities of water in the bulk and surface layer, respectively, and the surface layer has a thickness σ. The form of this function is shown in Figure 12, since the intercept at $Q = 0$ must be n_{s0} we can only adjust n_{s1} and σ to obtain agreement with the experimental data. The partial structure factor for this model is oscillatory in nature, the value of n_{s1} controlling the amplitude of the oscillations and σ controlling the frequency. From the experimental data in Figure 12 for $Q \geq 0.15$ Å^{-1}, the value of n_{s1} varies from ca. 0.031 to 0.025 Å^{-3} for Γ_s values of 0.3 and 2.0 mg m^{-2}, respectively. However, the uniform layer model does not reproduce the reduction observed in the experimental data at $Q \approx 0.03$ Å^{-1} without introducing strongly oscillatory features over the range of Q that is experimentally accessible. The water self-partial structure factor must be more complex than the original simple model. We note here that the reduction in the partial structure factors observed here is frequently (if not always) evident in other water self-partial structure factors where ethylene oxide residues are present in the surface layer either as a spread film[10,21,31] or an adsorbed layer. Any model must reproduce the correct

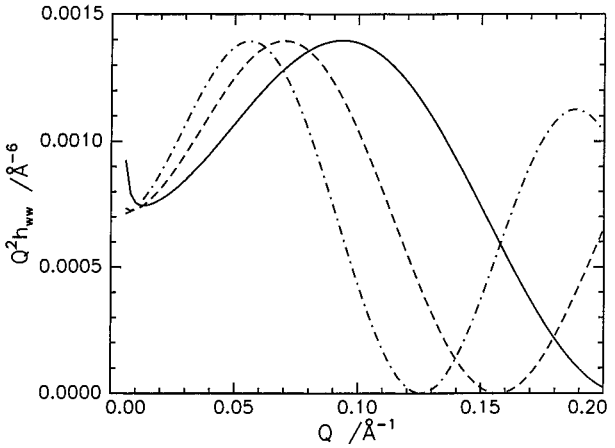

Figure 13. Self-partial structure factors data for water in the near surface layer calculated for a parabolic increase in water number density from the surface value (n_i) to the bulk value (n_{so}). For all curves $n_{so} = 0.033$ Å^{-3}; $n_i = 0.02$ Å^{-3}; solid line $d = 15$ Å, dashed line $d = 20$ Å, dot−dash line $d = 25$ Å.

value of n_{s0} (0.033 Å^{-3}) at $Q = 0$. A model with two different uniform layers of water near the surface preceding the bulk of the subphase fails to reproduce the observed data since the partial structure factor is again highly oscillatory over the Q range used. A third model that we have compared with the data is one where the water number density in the near surface layer has a parabolic increase over a finite length from a low value at the air−water interface to the number density corresponding to that of bulk water. Although this model has the qualitative features of the experimental data, see Figure 13, at high Q the model does not approach the values actually observed, a strong maximum appears before the decay to the intercept at $Q = 0$, and there is no evidence for this in the data. This parabolic model does not reproduce the features of the experimental data sufficiently well to justify any attempts to fit the data using it. The details concerning the organization of water in the neighborhood of poly(ethylene oxide) remain unresolved. It is abundantly clear that this organization is much more complex than the usual uniform layer model that has been used to model such data (but usually the Q range does not explore the low values used here). The key information is in principle obtainable from reflectivity at lower Q values than those used thus far, i.e., $Q < 0.02$ Å^{-1}; unfortunately for the D_2O subphase that would have to be used to collect the necessary data critical reflection intervenes at $Q \sim 0.017$ Å^{-1}, and no information concerning subphase distribution is obtainable.

Conclusions

A well-defined graft copolymer with a high density of poly(ethylene oxide) grafts has been spread at the air−water interface to form stable thin films. Neutron reflectometry has been used to determine the layer organization and the distribution of water in the near surface region occupied by the spread film. The hydrophobic backbone constitutes the majority of the uppermost layer, the minority component being air with some evidence of a very small amount of PEO also being present. This latter component is thought to arise from a combination of the cis/trans stereochemistry of the backbone and the strong affinity for the subphase of the PEO grafts resulting in some of the grafts bending over the backbone before being immersed in the aqueous subphase. Neutron reflectivity data have been analyzed by both the optical matrix method and a subset of the kinematic approximation approach, providing the partial structure factors for the PEO graft layer and the near surface water layer. Both analytical approaches show that the layer thickness of the PEO containing region increases as the surface concentration of the spread film increases. The increase in surface concentration produces an increase in grafting density of the air−water interface by the PEO grafts. The backbone-containing layer has a constant thickness of ca. 5 Å over the entire range of surface concentration explored. Number densities of PEO extracted from the most appropriate model fits to the reflectivity are able to account for 95−98% of the PEO actually spread on the water surface. As the surface concentration is increased, the reduction in separation distance between the PEO grafts is accompanied by an expulsion of water from the PEO-containing layer and a stretching of the grafts deeper into the subphase. The thickness of the PEO-containing region increases linearly with the grafting density at the water surface (assuming all PEO grafts become immersed). This behavior is predicted by the brush layer theories of Alexander and de Gennes as well as Milner, Witten, and Cates. However, the scaling exponent obtained experimentally is at least twice that predicted by theory. The differences between the situations for which the original theories were developed and that which prevails in the experiments have been cited as a possible cause for the discrepancy along with the modest length of the PEO grafts in the polymers investigated.

References and Notes

(1) Peace, S. K.; Richards, R. W.; Williams, N. *Langmuir* **1998**, *14*, 667.
(2) Booth, C.; Richards, R. W.; Taylor, M. R.; Yu, G. E. *J. Phys. Chem., B* **1998**, *102*, 2001.
(3) Richards, R. W.; Rochford, B. R.; Taylor, M. R. *Macromolecules* **1996**, *29*, 1980.
(4) Richards, R. W.; Taylor, M. R. *J. Chem. Soc., Faraday Trans.* **1996**, *92*, 601.
(5) Richards, R. W.; Taylor, M. R. *Macromolecules* **1997**, *30*, 3892.
(6) Brinkhuis, R. H.; Schouten, A. J. *Macromolecules* **1991**, *24*, 1496.
(7) Langevin, D. *Light Scattering by Liquid Surfaces and Complementary Techniques*; Marcel Decker: New York, 1992; Vol. 41.
(8) Jones, R. A. L.; Richards, R. W. *Polymers at Surfaces and Interfaces*; Cambridge University Press: Cambridge, England, 1999.
(9) Styrkas, D. A.; Thomas, R. K.; Adib, Z. A.; Davis, F.; Hodge, P.; Liu, X. H. *Macromolecules* **1994**, *27*, 5504.
(10) Peace, S. K.; Richards, R. W.; Taylor, M. R.; Webster, J. R. P.; Williams, N. *Macromolecules* **1997**, *31*, 1261.
(11) Thomas, R. K. Neutron Reflection from Polymer Bearing Surfaces. In *Scattering Methods in Polymer Science*; Richards, R. W., Ed.; Ellis Horwood: London, 1995.
(12) Penfold, J.; Thomas, R. K. *J. Phys.: Condens. Matter* **1990**, *2*, 1369.
(13) Russell, T. P. *Mater. Sci. Rep.* **1990**, *5*, 171.
(14) Lu, J. R.; Simister, E. A.; Thomas, R. K.; Penfold, J. *J. Phys. Chem.* **1993**, *97*, 6024.
(15) Lu, J. R.; Simister, E. A.; Lee, E. M.; Thomas, R. K.; Rennie, A. R.; Penfold, J. *Langmuir* **1992**, *8*, 1837.
(16) Nguyen, S. T.; Johnson, L. K.; Grubbs, R. H. *J. Am. Chem. Soc.* **1992**, *114*, 3971.
(17) Heroguez, V.; Breunig, S.; Gnanou, Y.; Fontanille, M. *Macromolecules* **1996**, *29*, 13.
(18) Feast, W. J.; Gibson, V. C.; Johnson, A. F.; Khosravi, E.; Mohsin, M. A. *J Mol. Catal. A: Chem.* **1997**, *115*, 37.
(19) Barth, H. G.; Mays, J. W. *Modern Methods of Polymer Characterisation*; Wiley: New York, 1991.
(20) Hamilton, J. G. *Polymer* **1998**, *39*, 1669.

(21) Henderson, J. A.; Richards, R. W.; Penfold, J.; Thomas, R. K.; Lu, J. R. *Macromolecules* **1993**, *26*, 4591.
(22) Daoud, M.; Jannink, G. *J. Phys. (Paris)* **1975**, *37*, 973.
(23) Kawaguchi, M. *Prog. Polym. Sci.* **1993**, *18*, 341.
(24) Vilanove, R.; Rondelez, F. *Phys. Rev. Lett.* **1980**, *45*, 1502.
(25) Miller, A. F.; Richards, R. W. Unpublished results.
(26) Crowley, T. L.; Lee, E. M.; Simister, E. A.; Thomas, R. K.; Penfold, J.; Rennie, A. R. *Colloids Surf.* **1990**, *52*, 85.
(27) Alexander, S. *J. Phys. (Paris)* **1977**, *38*, 977.
(28) de Gennes, P. G. *Macromolecules* **1980**, *13*, 1069.
(29) Milner, S. T.; Witten, T. A.; Cates, M. E. *Macromolecules* **1988**, *21*, 2610.
(30) Milner, S. T.; Witten, T. A.; Cates, M. E. *Macromolecules* **1989**, *22*, 853.
(31) S K Peace, S. K.; Richards, R. W.; Kiff, F. T.; Webster, J. R. P.; Williams, N. *Polymer* **1998**, *40*, 207.

MA000205S